 doi:10.20944/preprints202211.0105.v1

*Article*

# High-Iron Bauxite Residue (Red Mud) Valorisation Using Hydrochemical Conversion of Goethite to Magnetite

**Andrei Shoppert [1,2,*], Dmitry Valeev [3], Mamodou Malal Diallo [1], Irina Loginova [1], Marie Constance Beavogui [4], Abdukhakim Rakhmonov [2], Yevgeniy Ovchenkov [5] and Denis Pankratov [6]**

[1] Department of Non-Ferrous Metals Metallurgy, Ural Federal University, 620002 Yekaterinburg, Russia; i.v.loginova@urfu.ru (I.L.); malalkoura2@gmail.com (M.M.D.)
[2] Laboratory of Advanced Technologies in Non-Ferrous and Ferrous Metals Raw Materials Processing, Ural Federal University, 620002 Yekaterinburg, Russia; a.a.rakhmonov@urfu.ru (A.R.)
[3] Laboratory of Sorption Methods, Vernadsky Institute of Geochemistry and Analytical Chemistry of the Russian Academy of Sciences, 119991 Moscow, Russia; dmvaleev@yandex.ru
[4] Laboratoire de Recherche Appliquée en Géoscience et Environnement, Institut Supérieur des Mines et Géologie de Boké (ISMGB), Boke, Guinea; beavoguimarie11@gmail.com
[5] Department of Physics, Lomonosov Moscow State University, 119991 Moscow, Russia; ∗ovtchenkov@mig.phys.msu.ru
[6] Department of Chemistry, Lomonosov Moscow State University, 119991 Moscow, Russia; pankratov.denis@gmail.com
* Correspondence: a.a.shoppert@urfu.ru

**Abstract:** Bauxite residue (BR), also known as red mud, is a by-product of the production of alumina via the Bayer process. Because of the high sodium oxide and other impurities content, this material is not used to obtain iron or other iron-containing products. In this paper, the hydro-chemical conversion of goethite (FeOOH) to magnetite ($Fe_3O_4$) in high-iron BR from the Friguia alumina refinery (Guinea) by $Fe^{2+}$ ions in highly concentrated alkaline media was studied. The simultaneous extraction of Al and Na made it possible to obtain a product containing more than 96% $Fe_3O_4$. The results show that the magnetization of Al-goethite and Al-hemetite accelerates the dissolution of the Al from the iron mineral solid matrix and from the desilication product (DSP). After ferrous sulfate ($FeSO_4 \cdot 7H_2O$) was added directly at the $FeO:Fe_2O_3$ molar ratio of 1:1 at 120 °C for 150 min in the solution with the 360 g $L^{-1}$ $Na_2O$ concentration, the alumina extraction ratio reached 96.27% for the coarse bauxite residue size fraction (Sands) and 87.06% for fine BR obtained from red mud. The grade of iron (total iron in the form of iron element) in the residue can be increased to 69.55% for Sands and 58.31% for BR. The solid residues obtained after leaching were studied by XRD, XRF, TG-DTA, VSM, Mössbauer spectroscopy and SEM to evaluate the conversion and leaching mechanisms and the recovery ratio of Al from different minerals. The iron-rich residues can be used in the steel industry or as a pigment.

**Keywords:** alkali leaching; red mud; high-iron waste; disposal; Al-goethite; conversion; magnetite

## 1. Introduction

BR is a solid fraction of the red mud. Each year, over 150 million tons of red mud are produced during the Bayer process, which is used to extract Al from bauxites by the alkaline method [1]. Because of this method, red mud has a high amount of caustic alkali and other impurities, which makes it very toxic [2]. Moreover, the concentration of heavy metals in BR can be doubled after alumina extraction [3,4]. The utilization rate of BR is very low because of its high toxicity and corrosivity [5–7].

BR has a high number of valuable components, such as iron, rare earth elements (REEs), vanadium, titanium, etc. [8–14]. The extraction of these elements from BR together with the reduction of its toxicity can be economically and ecologically beneficial. For example, BR produced from the Fria bauxite deposit in Guinea has a very high amount of iron: 40% of the iron in red mud obtained after digestion of bauxites on the Friguia

 doi:10.20944/preprints202211.0105.v1

alumina refinery, or 55-60% of the iron in the sands obtained by the gravity method of separation of BR before thickening and washing step [15].

Different methods of iron production from BR have been studied so far. These methods can be divided into pyro- and hydrometallurgical [16]. Pyrometallurgical methods include magnetic separation after preliminary reductive roasting [17], reductive sintering with different fluxes [18,19], and smelting BR with a reducing agent to make pig iron [20,21]. The major disadvantage of these methods is their high energy consumption, since the temperatures of these processes can reach as high as 1000-1750 °C [22].

Li et al. [23,24] and Pasechnik et al. [25] showed that hematite from BR can be converted into magnetite during a hydrothermal reduction in the presence of iron powder, $Fe^{2+}$, and $OH^-$ ions (Equation (1)-(3)). However, a high-pressure process with a leaching temperature greater than 250 °C is required for complete iron conversion into magnetite.

$$Fe + H_2O + OH^- = HFeO_2^- + H_2, \quad (1)$$

$$Fe^{2+} + 3OH^- = HFeO_2^- + H_2O, \quad (2)$$

$$Fe_2O_3 + HFeO_2^- = Fe_3O_4 + OH^-. \quad (3)$$

Furthermore, Zhou et al. [26] showed that the addition of Al during high-temperature digestion of high-iron bauxite not only transforms iron into hematite covered by magnetite but also accelerates Al extraction from Al-goethite that is hard to dissolve by the Bayer method. However, a high-pressure leaching at 270 °C is required for the formation of the iron-enriched residue with an iron content of 56%. Such iron content is still very low, especially if the pigment-quality magnetite is proposed as a final product.

Vu et al. [27] and Bohacek et al. [28] proposed a method for the production of black pigment-quality magnetite from jarosite ($NH_4Fe_3(SO_4)_2(OH)_6$) by decomposition in an ammonia or sodium alkali environment in the presence of ferrous sulfate (Equations (4) and (5)). The mixture was then heated to 90 °C and maintained for 7 h to obtain a well-crystallized product with iron content higher than 70% [27].

$$NH_4Fe_3(SO_4)_2(OH)_6 + 2OH^- \rightarrow NH_4^+ + 3Fe(OH)_3 + 2SO_4^{2-}, \quad (4)$$

$$2Fe(OH)_3 + Fe^{2+} + 2OH^- \rightarrow Fe_3O_4 + 4H_2O, \quad (5)$$

This freshly precipitated $Fe(OH)_3$ is very reactive, so magnetite can be formed at a lower temperature (90 °C vs. 250 °C for hematite in bauxites). Hage et al. [29] suggested a method for making magnetite from jarosite using MgO as a neutralizing agent and acid-treated cellulose as a reductant. Using a reducing agent saves expensive alkali, which is neutralized and turned into $Na_2SO_4$ by adding $FeSO_4$. Both methods allow for the obtainment of high-quality magnetite products from jarosite that itself has very low impurities.

In this work, a novel method of atmospheric pressure leaching (APL) of Guineas high-iron BR in the presence of $FeSO_4$ was proposed, which led to almost complete dissolution of Al from the solid matrix of the sands with the formation of the pigment-quality magnetite containing about 70% of Fe. The extraction of Al from the red mud was also higher than 87%, however, the iron content in the solid residue reached only 58 %. The optimum conditions of alumina extraction and iron minerals conversion as well as the mechanism of these processes were verified. The solids were examined using X-ray diffraction (XRD), X-ray fluorescence (XRF), Scanning electron microscopy with energy dispersive spectroscopy (SEM-EDS), Mossbauer spectrometry, Vibrating sample magnetization (VSM), and spectrophotometry methods.

 doi:10.20944/preprints202211.0105.v1

## 2. Materials and Methods

### *2.1. Chemical composition of samples*

The chemical composition of the raw BR and residues after leaching were analyzed using a powder X-ray fluorescence spectrometry with an Axios MAX spectrometer (Malvern Panalytical Ltd., Almelo, Netherlands). Tablet-shaped samples (Ø 20 mm; 300 mg) were prepared for analysis via pressing. Also, polystyrene was used as a binder at a ratio of 5:1. Super Q software was used to calculate the metallic contents of the samples.

The Sc content in BR and sands leaching residues were determined by inductively coupled plasma mass spectrometry (ICP-MS) using an X Series II quadrupole mass spectrometer (Thermo Scientific, Germany). The quantitative determination of the Sc was carried out using iPlasmaProQuad software (GEOKHI RAS, Moscow, Russia)

### *2.2. Phisical properties of samples*

The phase composition of the raw BR and residues after leaching was analyzed using X-ray diffraction using a Difrei-401 diffractometer (JSC Scientific Instruments, Saint Petersburg, Russia) using a Cr-K$\alpha$ radiator with 2$\theta$ angles ranging from 15° to 140°. The X-ray source operated with an output of 25 kW and an exposure time of 30 min. The diffraction data were processed using the Match 3! (Crystal Impact GmbH, Bohn, Germany) software. The particle size distribution of the samples was measured with a SALD-2201 Laser Diffraction Particle Size Analyser (Shimadzu, Kyoto, Japan). The surface morphology and elemental mapping of the raw materials and the residues were investigated using SEM–EDX methods on a Vega III microscope (Tescan, Brno, Czech Republic). The Mössbauer analysis of raw BR and sands, residues after leaching were done using a spectrometer MS1104EM (Cordon, Rostov-on-Don, Russia) at 296±3 K and 77.6±0.5 K temperature in a vacuum cryostat. The $^{57}$Co nuclei in Rh matrix with 3 mCi activity (RITVERC, Saint Petersburg, Russia) was used as the $\gamma$-radiation source. The SpectrRelax 2.8 software (Lomonosov Moscow State University, Moscow, Russia) was used to analyze the Mössbauer spectra. Values of chemical shifts are presented relative to $\alpha$-Fe. The magnetic measurements were performed using a MPMS-XL-7 SQUID magnetometer (Quantum Design, San Diego, California, USA). The TG-DTA analysis was performed using simultaneous thermogravimetry analyzer STA 449 F3 Jupiter (Netzsch, Selb, Germany). over a range of 33–1100 °C at a heating rate of 10 °C min$^{-1}$. An air atmosphere was used, with a flow rate of 20 ml min$^{-1}$.

### *2.3. Materials*

The bauxite residue and sands used in this research were obtained from Friguia alumina refinery in Guinea with GPS coordinates N10.39°, W13.58°. Sands are the coarser particles of residue obtained from red mud by separation through hydrocyclones before the thickening and washing step. The chemical compositions of BR and the sands are presented in Table 1. Figure 1 shows the particle size distribution of samples. It is obvious that sands obtained using a hydrocyclone separator are significantly coarser than BR, and the particle size distribution of the sands is more uniform. Figure 2 shows the morphology and elemental mapping of the samples. BR is composed of particles smaller than 10 μm, and the Fe, Na, Si, and Al elemental mapping are similar, which can be explained by the precipitation of DSP and gibbsite during the thickening and washing steps. The sands elemental map shows that there are a lot of goethite particles and some single aluminum particles with a small amount of silicon and sodium and a lot of iron on the surface. This implies that desilication of the solution is ending during the thickening and washing stage. The re-precipitation of gibbsite from a diluted aluminate solution during the washing step also leads to a higher concentration of aluminum in the BR.

The other reagents, NaOH and $FeSO_4 \cdot 7H_2O$, were of analytical grade. Sodium alkaline solutions with a $Na_2O$ concentration of 330-400 g L$^{-1}$ were obtained by mixing NaOH with distilled water.

Preprints (www.preprints.org) | NOT PEER-REVIEWED | Posted: 7 November 2022 doi:10.20944/preprints202211.0105.v1

**Table 1.** The chemical compositions of bauxite residue (BR) and sands from Friguia alumina refinery, Guinea, wt. %.

| Sample | Fe | Si | Ti | Al | Na | O | Other |
|---|---|---|---|---|---|---|---|
| BR | 41.7 | 4.25 | 4.36 | 12.34 | 4.53 | 30.68 | 2.14 |
| Sands | 56.23 | 0.77 | 1.38 | 5.55 | 1.26 | 33.80 | 1.01 |

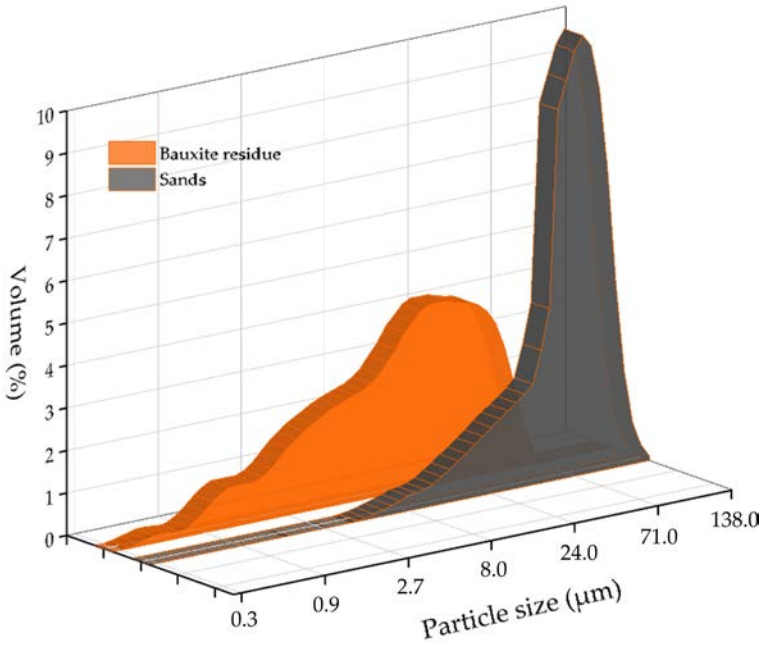


**Figure 1.** The particle size distribution of the bauxite residue (BR) and sands from the Friguia alumina refinery.

*2.4. Experimental*

The extraction of Al with NaOH and the conversion of goethite to magnetite were carried out in the thermostated 0.5 L stainless steel reactor. The reactor has openings for stirring as well as for controlling temperature and recycling evaporated water through a water-cooled condenser. The L:S ratio and the stirring speed in all experiments were 100 g $L^{-1}$ and 300 rpm, respectively. The molar ratio of $Fe^{2+}$ added in the form of iron sulphate to $Fe_2O_3$ in BR or sands according to Equation (3) was equal to 1.0. The BR, sands, and iron sulphate were added to a hot solution with a $Na_2O$ concentration of 330 g $L^{-1}$ to 400 g $L^{-1}$. This made it possible to use the atmospheric leaching process at a temperature of 120 °C. The temperature of the leaching was varied from 100 to 120 °C, and the leaching time from 1 to 5 h. After leaching, the pulp was filtered, and the solid residue was dried at 110 °C for 8 h before analysis.

*2.5. Experimental data calculation*

In order to avoid the mutual influence of factors on each other and to reduce the number of experiments, a Box-Benken experimental design created in the Statistica 13 software (TIBCO, Hamburg, Germany) was used in this research. The design consists of three blocks of fifteen experiments each, with varying parameters at three levels. The output parameters are the extraction of aluminum into solution and the concentration of iron in the solid residue.

Preprints (www.preprints.org) | NOT PEER-REVIEWED | Posted: 7 November 2022 doi:10.20944/preprints202211.0105.v1

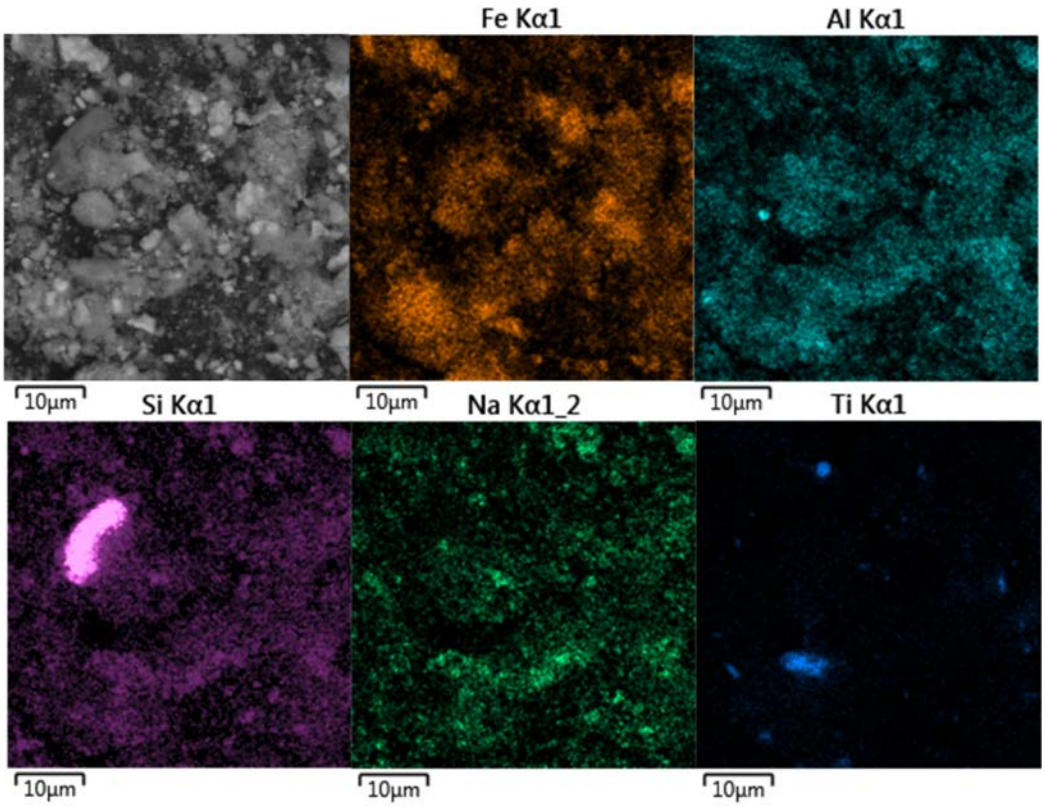


(**a**)

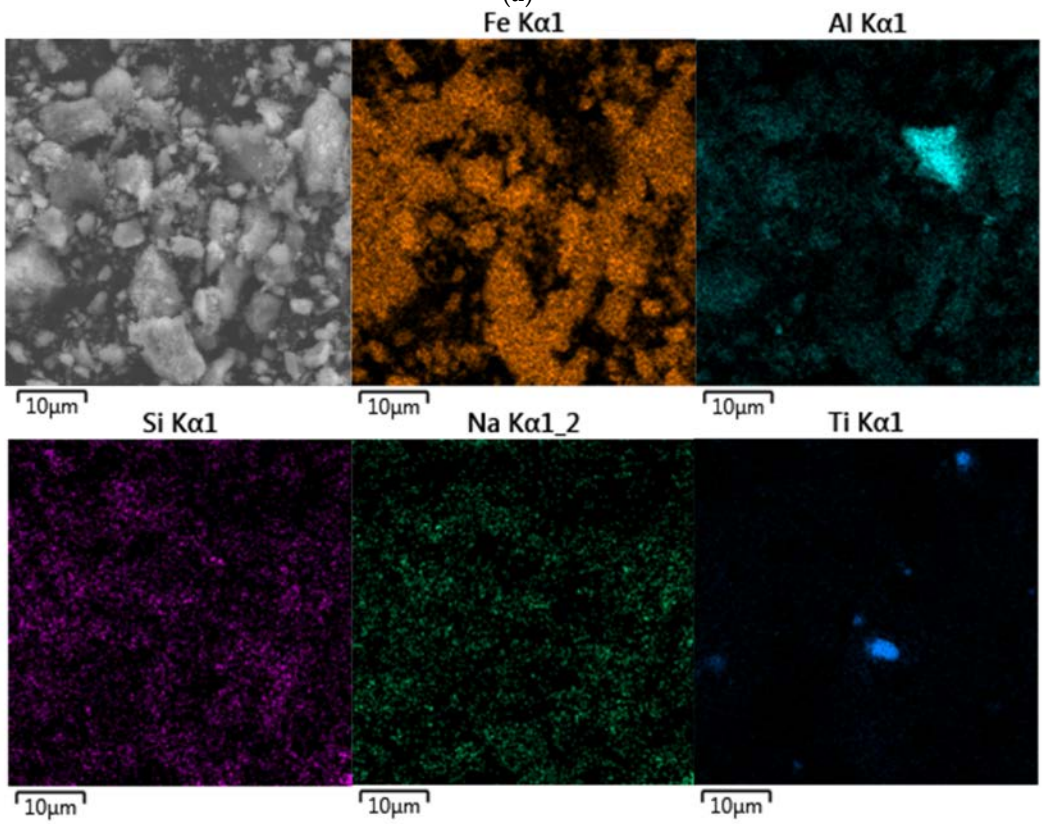


(**b**)

**Figure 2.** BSE image and elemental mapping of the BR particles surface (a); BSE images and elemental mapping of the sands particles surface (b).

The statistical-based automated neural network (SANN) was used for modeling the Al and Fe extraction and $Na_2O$ concentration in the solid residue. SANN is an artificial

Preprints (www.preprints.org) | NOT PEER-REVIEWED | Posted: 7 November 2022 doi:10.20944/preprints202211.0105.v1

intelligence-based method that adjusts the result of modeling until the desired quality is obtained. Statistica 13 was used to make SANN models using a multilayer perceptron (MLP) method.

The amount of Al that was extracted from the different aluminum minerals (X) into the solution was estimated using Equation (6):

$$X = (m_1 \times X_1 - m_2 \times X_2)/ (m_1 \times X_1), \quad (6)$$

where $m_1$ – the mass of the original sample, [g]; $X_1$ – mineral content in the original sample, [%], $m_2$ – the mass of the leaching residue, [g]; $X_2$ – mineral content in the leaching residue, [%].

To assess the content of Na in the raw materials and solid residue, we used the assumption that all the Na in the product is represented by DSP (equation (7):

$$DSP = [(Na \times 23) / (27 \times Al)] \times 100\%, \quad (7)$$

where Na – the content of sodium in a sample, [%]; Al – the Al content in a sample, [%]; 23/27 – the molar ratio of Na vs Al in the sodalite.

In the case of sands that have only two Al minerals, the equation (8) was used to calculate the aluminum contained in solid matrix:

$$\text{Solid matrix}_{sands} = [(Al - DSP) / Al] \times 100\%, \quad (8)$$

where Al – the Al content[20] in a sample, [%]; DSP – the amount of Al in the DSP in this sample calculated by equation (7), [%].

To determine the amount of aluminum hydroxides in the solid matrix of BR iron minerals, we assumed that the amount of this Al has a linear dependence on the Fe content in the residue (Equation (9):

$$\text{Solid matrix}_{BR} = [(\text{Solid matrix}_{sands} \times Fe_{BR}) / Fe_{sands}] \times 100\%, \quad (9)$$

where $\text{Solid matrix}_{sands}$ – the amount of Al in the solid matrix of the raw sands iron minerals calculated by equation (8), [%]; $Fe_{BR}$ – the Fe content in the BR, $Fe_{sands}$ – the Fe content in the raw sands, [%].

Therefore, all the remaining Al in the BR is represented by the reprecipitated gibbsite.

The blackness (jetness) evaluation was made using an SR-60 colorimeter (Shenzhen ThreeNH Technology Co., Shenzhen, China). To obtain a single numerical result, the calculation of the magnitude of the blackness (My) was based on one of the values of the color coordinates - L (brightness) that was determined by Equation (10):

$$My=100 \times \log(100 / L). \quad (10)$$

This only determines how light or dark the sample is without taking the color shade into account. Since the shade of black affects how dark something looks, the degree of jetness (Mc) was determined by changing CIE LAB results to CMYK in the color model with the following equation (11):

$$M_c=100 \times ((\log(X_n / X) - \log(Y_n / Y) + \log(Z_n / Z)). \quad (11)$$

The Mc value describes a higher blackness if the shade is blue (Z), and a lower saturation if the shade is yellow (Y). $X_n$, $Y_n$, $Z_n$ - standard color values of the illuminating light type.

Preprints (www.preprints.org) | NOT PEER-REVIEWED | Posted: 7 November 2022 doi:10.20944/preprints202211.0105.v1

## 3. Results and discussion

### *3.1. The nature of the Al-containing phase in the raw materials*

Previous research by Zhou et al. [26] showed that the rate of Al extraction from Guinea's bauxite with a high iron content is limited by the presence of aluminum substituted goethite (Al-goethite), which is refractory using conventional Bayer process conditions. To study the occurrence of Al in the BR and the Sands from the Friguia alumina refinery, the phase composition of the samples was studied using XRD, TGA and Mössbauer spectrometry. The XRD patterns of the BR and the Sands are shown in Figure 3. Figures 6a and 6b indicate that there are differences in hematite, goethite and gibbsite content in the raw BR and sands. The peaks of goethite are higher in the sand samples, whereas hematite is found in higher concentrations in the BR. Additionally, there are peaks of sodalite (DSP) in the BR that are not seen in the sands due to the low content.

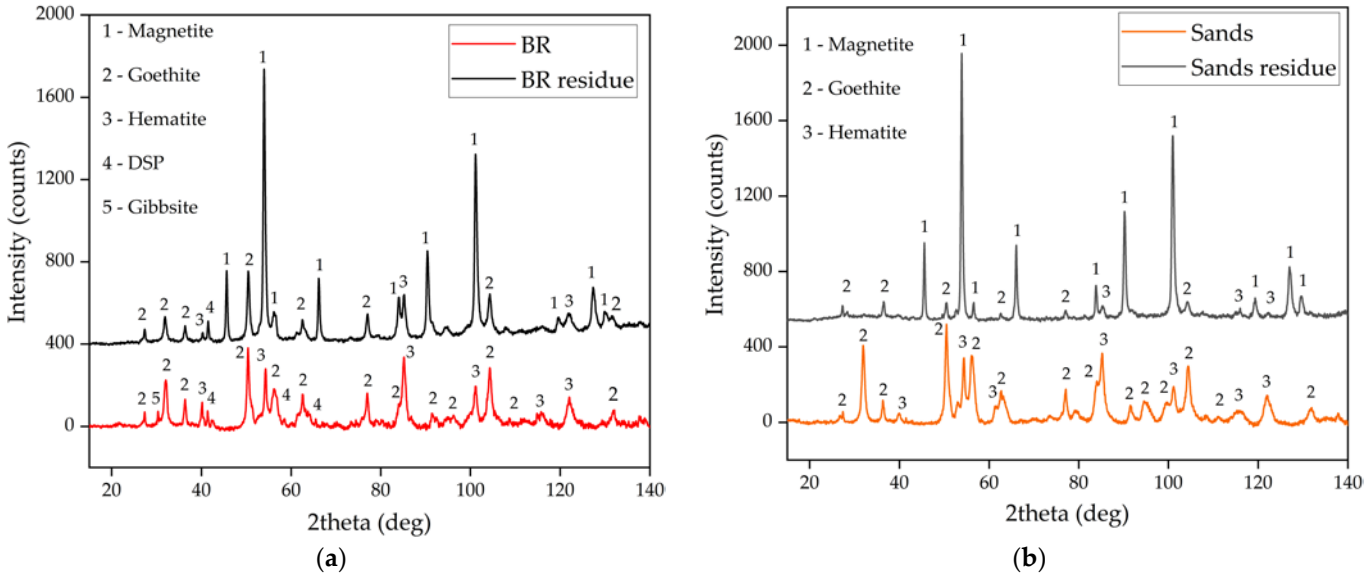


**Figure 3.** The XRD patterns of the BR and the solid residue obtained after BR leaching at the optimal conditions (a); the XRD patterns of the Sands and the solid residue obtained after Sands leaching at the optimal conditions (b).

Figure 4 shows the TG-DTA curves of the BR and the Sands. There are significant differences in the DTA of these two samples. Figure 4a shows that the decomposition of BR occurred in five stages, similar to the results obtained by Zhou et al. [30] for Al-goethite containing bauxite residues. The 1st stage (from 25 to 220 °C) is attributed to the loss of moisture [21]. The 2nd stage (from 220 to 330 °C) with the endothermic peak at 299.1 °C is associated with the decomposition of gibbsite [31]. The 3rd stage occurred at temperatures between 330 and 370 °C, and an endothermic peak of goethite and al-goethite decomposition was found at 335.5 °C [32]. Between 335 and 420 °C the 4th stage, the boehmite undergoes decomposition. And the 5th stage with an endothermic peak of hydrosodalite decomposition was found at 495 °C [33]. The TG-DTA curve of the sands shows only endothermic peaks of goethite at 344.3 °C and a much smaller peak of hydrosodalite at 504.8 °C. These findings indicate that there is practically no gibbsite in the Sands and all aluminum is enclosed in a solid matrix of minerals and DSP.

Preprints (www.preprints.org) | NOT PEER-REVIEWED | Posted: 7 November 2022 doi:10.20944/preprints202211.0105.v1

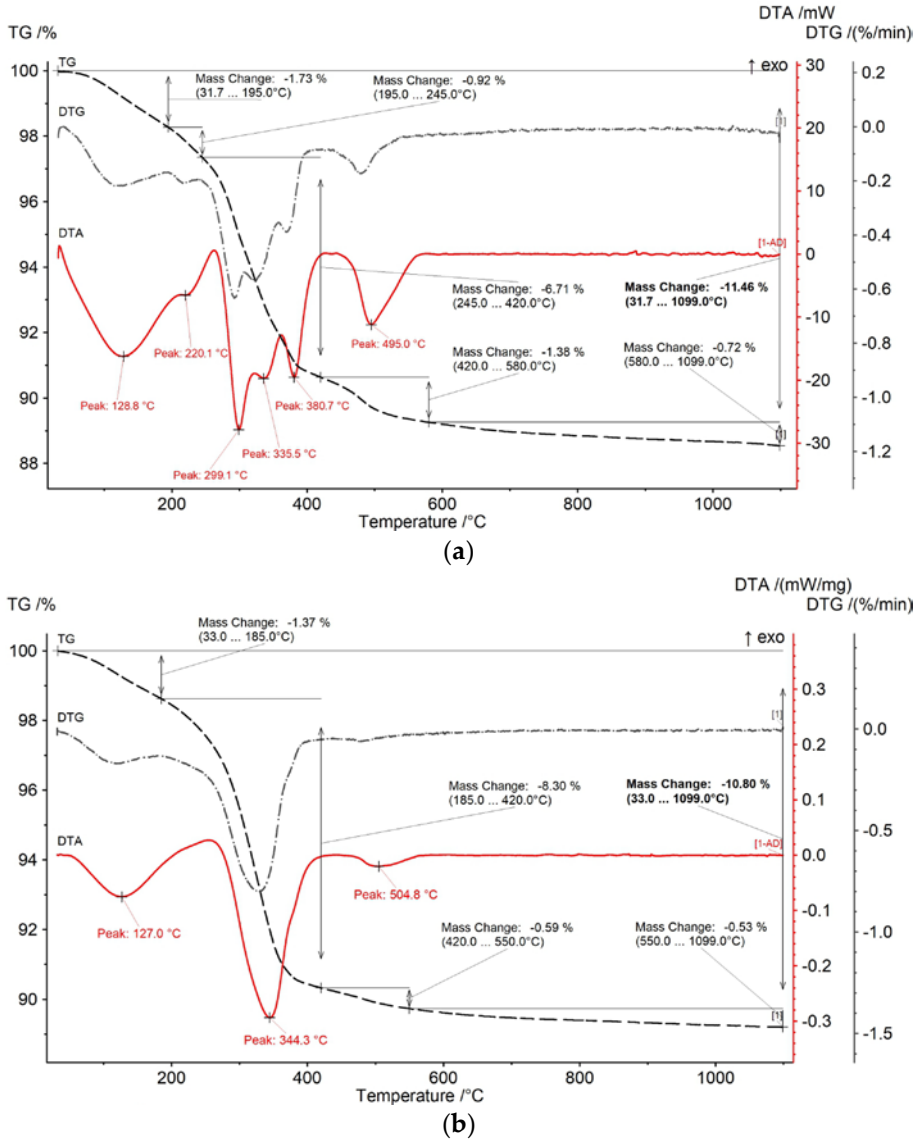


**Figure 4.** The TG-DTA curves of the BR (a); and Sands (b) at different temperatures.

Figure 5 shows that the results of the Mössbauer analysis of raw BR and Sands. - Samples at room temperature have a similar profile and are combinations of an intense paramagnetic doublet and a sextet with fairly narrow resonance lines (Figure 5). A noticeable difference between the spectrum of the Sands sample and BR is that the first sample has extended absorption between the first and fifth lines of the sextet (Figure 5a and 5c)). At the boiling point of nitrogen, the shape of the spectra changes significantly: the doublet almost completely disappears, and the outer lines of the narrow sextet split in pairs (Figure 5b and 5d)). All this testifies to the complex composition of the materials.

The Mössbauer spectra of the raw materials can be described by a superposition of four sextets and two doublets (Figure 5, Table 2). Two outer sextets at 296 K and one outer sextet at 78 K correspond to aluminum-substituted hematite – $\alpha$-$(Fe_{1-x}Al_x)_2O_3$ [34]. The low value of magnetic splitting even for frozen samples, and the absence of the Morin transition (TM=260 K for $\alpha$-$Fe_2O_3$) do not allow us to attribute these subspectra to pure unsubstituted hematite - $\alpha$-$Fe_2O_3$ [22,35]. The isomorphic substitution of aluminum for iron atoms [36] leads to a decrease in the effective magnetic field recorded in the spectra by approximately 1 kOe by 1 w.% for 300 K [37,38]. Analyzing the data presented in [38], it can be shown that the degree of substitution x in alumina hematite – $\alpha$-$(Fe_{1-x}Al_x)_2O_3$ can be expressed in terms of the effective magnetic field at room temperature, as:

Preprints (www.preprints.org) | NOT PEER-REVIEWED | Posted: 7 November 2022 doi:10.20944/preprints202211.0105.v1

$$x = 5.4982 - 0.0107*Heff, \quad (12)$$

Then, based on the experimental data (Table 2) for the studied samples using Equation (12), it is possible to determine the composition of Al-hematite as $\alpha$-$(Fe_{0.9}Al_{0.1})_2O_3$ for the 1st subspectrum, and $\alpha$-$(Fe_{0.7}Al_{0.3})_2O_3$ for the 2nd subspectrum (Table 2).

The next pair of sextets poorly resolved at room temperature, upon cooling to the boiling point of nitrogen, transforms into a pair of well-defined sextets with parameters close to goethite [39]. The reason for the low value of the effective magnetic field even at low temperatures is the partial replacement of iron atoms by aluminum, with the formation of Al-goethite – $\alpha$-$Fe_{1-x}Al_xOOH$, for which the temperature transformations of the spectrum are discussed in detail in [16].

The paramagnetic part of the high-temperature Mössbauer spectra may have a dual nature. On the one hand, 7-10% of the area of this pair of doublets can be related to the superparamagnetic fractions of the above described Al-hematite and Al-goethite [40]. The remaining part, as shown in [16] refers to akageneite substituted by aluminum – β-$Fe_{1-x}Al_xO$(OH, Cl), which, when cooled to the boiling point of nitrogen transforms into a broadened sextet (Table 2).The remaining minor components in the low-temperature spectra in the form of doublets correspond to $Fe^{3+}$ ions in the high-spin state and octahedral oxygen environment [41], which can isomorphically replace $Al^{3+}$ ions [36] in the crystal lattice of, for example, sodalite [42].

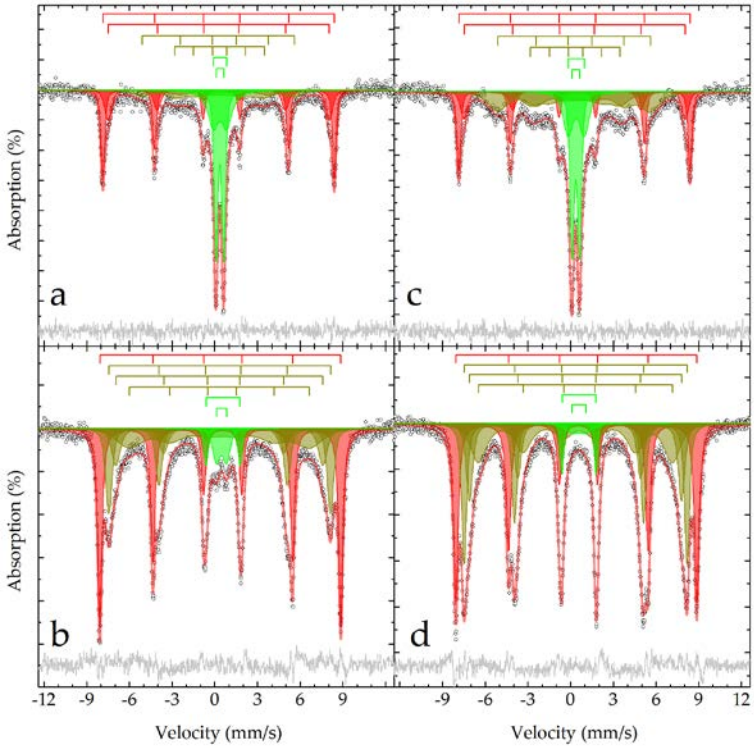


**Figure 5.** Mössbauer spectra obtained at 296 K (a, c) and 77.6 K (b, d) of the BR (a, b) and Sands (c, d) samples and their model description according to Table 2.

Based on the chemical analysis and the phase composition of the raw materials, the distribution of aluminum by minerals was calculated. Table 3 shows the results of the semi-quantitative calculation of the aluminum containing phase composition.

Preprints (www.preprints.org) | NOT PEER-REVIEWED | Posted: 7 November 2022 doi:10.20944/preprints202211.0105.v1

**Table 2.** The subspectrum parameters describing experimental Mössbauer spectra obtained at different temperatures for BR and Sands samples.

| Sample | | | BR | | | | | Sands | | | | |
|---|---|---|---|---|---|---|---|---|---|---|---|---|
| Temperature, K | Phase | № | δ | ε (Δ=2ε) | $\Gamma_{exp}$ | $H_{eff}$ | S | δ | ε (Δ=2ε) | $\Gamma_{exp}$ | $H_{eff}$ | S |
| | | | mm/s | | | kOe | % | mm/s | | | kOe | % |
| 296 | $\alpha$-$(Fe_{1-x}Al_x)_2O_3$ | 1 | 0.37±0.01 | -0.10±0.01 | 0.34±0.01 | 504.7±0.2 | 26±1 | 0.37±0.01 | -0.10±0.01 | 0.36±0.01 | 504.1±0.3 | 19±1 |
| | | 2 | 0.37±0.01 | -0.09±0.01 | 0.59±0.03 | 482±1 | 15±1 | 0.36±0.01 | -0.08±0.01 | 0.58±0.04 | 482±2 | 11±1 |
| | $\alpha$-$Fe_{1-x}Al_xOOH$ | 3 | 0.45±0.01 | -0.21±0.01 | 1.60±0.01 | 332.1±0.1 | 10±1 | 0.45±0.05 | -0.21±0.05 | 1.60±0.09 | 332±2 | 23±1 |
| | | 4 | 0.32±0.01 | -0.01±0.01 | 1.60±0.01 | 195.5±0.1 | 11±2 | 0.32±0.07 | -0.01±0.05 | 1.60±0.09 | 196±4 | 15±1 |
| | β-$Fe_{1-x}Al_xO$(OH, Cl) | 5 | 0.37±0.01 | (1.0±0.3) | 0.88±0.07 | | 15±5 | 0.39±0.01 | (1.1±0.1) | 0.84±0.09 | | 12±2 |
| | | 6 | 0.36±0.01 | (0.53±0.01) | 0.33±0.03 | | 23±5 | 0.36±0.01 | (0.52±0.01) | 0.36±0.01 | | 19±2 |
| 77.6 | $\alpha$-$(Fe_{1-x}Al_x)_2O_3$ | 1 | 0.48±0.01 | -0.08±0.01 | 0.37±0.01 | 525.2±0.1 | 38.4±0.7 | 0.47±0.01 | -0.07±0.01 | 0.40±0.01 | 525.1±0.1 | 31.8±0.5 |
| | $\alpha$-$Fe_{1-x}Al_xOOH$ | 2 | 0.47±0.01 | -0.12±0.01 | 0.56±0.01 | 482.9±0.4 | 22±1 | 0.47±0.01 | -0.12±0.01 | 0.43±0.01 | 485.5±0.2 | 24.9±0.9 |
| | | 3 | 0.47±0.01 | -0.15±0.01 | 0.75±0.04 | 451±1 | 13±1 | 0.47±0.01 | -0.13±0.01 | 0.56±0.02 | 461.8±0.5 | 18±1 |
| | β-$Fe_{1-x}Al_xO$(OH, Cl) | 4 | 0.40±0.04 | -0.09±0.03 | 2.18±0.01 | 391.6±0.1 | 19.0±0.5 | 0.47±0.01 | -0.14±0.01 | 1.34±0.04 | 422±2 | 21±1 |
| | $Fe^{3+}_{Oh}$ (DSP) | 5 | 0.59±0.01 | (2.37±0.01) | 0.33±0.02 | | 2.9±0.1 | 0.59±0.01 | (2.38±0.01) | 0.25±0.01 | | 2.5±0.2 |
| | | 6 | 0.47±0.01 | (0.71±0.02) | 0.62±0.03 | | 4.8±0.2 | 0.57±0.05 | (1.0±0.1) | 1.2±0.3 | | 2.0±0.3 |

$\delta$ – Isomer shift; ε (Δ) - Quadrupole shift (splitting); $\Gamma_{exp}$ – Line width; $H_{eff}$ – Hyperfine magnetic field; $S$ – Relative area of a subspectrum №.

**Table 3.** The results of the semi-quantitative calculation of the aluminum containing phase composition in the BR and the sands, wt. %.

| Sample | Desilication product | Aluminum hydroxide in the solid matrix | Re-precipitated gibbsite |
|---|---|---|---|
| BR | 31.3 | 26.7 | 42.0 |
| Sands | 19.3 | 80.7 | - |

*3.2. The effect of leaching parameters on the Al extraction and the Fe, Na content in the solid residue*

To see how different leaching parameters affect the rate of Al extraction and the Fe, $Na_2O$ content in the solid residue, the experiments were done according to the method described in section 2.5. Using the experimental results, a neural network model of the process was obtained. Figure 6 shows the response surfaces of the model constructed by varying time, temperature, and the $Na_2O$ concentration of the solution in the leaching process of the BR.

The major effect on Al extraction degree (Figure 6a and Figure 6b) is caused by leaching time and temperature. Figure 6a shows that before 2.0-3.5 h of leaching, the Al extraction degree is increasing. After 3.5 h at 100 °C and 3 h at 110 °C, Al begins to precipitate in the form of desilication product (DSP), which can be confirmed by the increased content of $Na_2O$ in the solid residue after 4 h of leaching (Figure 6e and Figure 6f). After 4 hours of leaching, the iron content in the solid residue decreases because of the DSP precipitation (Figure 6c and Figure 6d). Nevertheless, a high Al extraction degree was achieved after 2 h at all leaching temperatures – more than 80%. After 2.5 hours of leaching at T = 120 °C, the total Fe content in the solid residue can be increased from 41.7% (Table 1) to 56%. The $Na_2O$ concentration in the solution did not have a significant effect on the Al extraction and the Fe, $Na_2O$ content in the solid residues (Figure 6b, 6d, 6f). Therefore, the effect of $Na_2O$ concentration in the solution on the sands leaching is not shown (Figure 7).

Preprints (www.preprints.org) | NOT PEER-REVIEWED | Posted: 7 November 2022 doi:10.20944/preprints202211.0105.v1

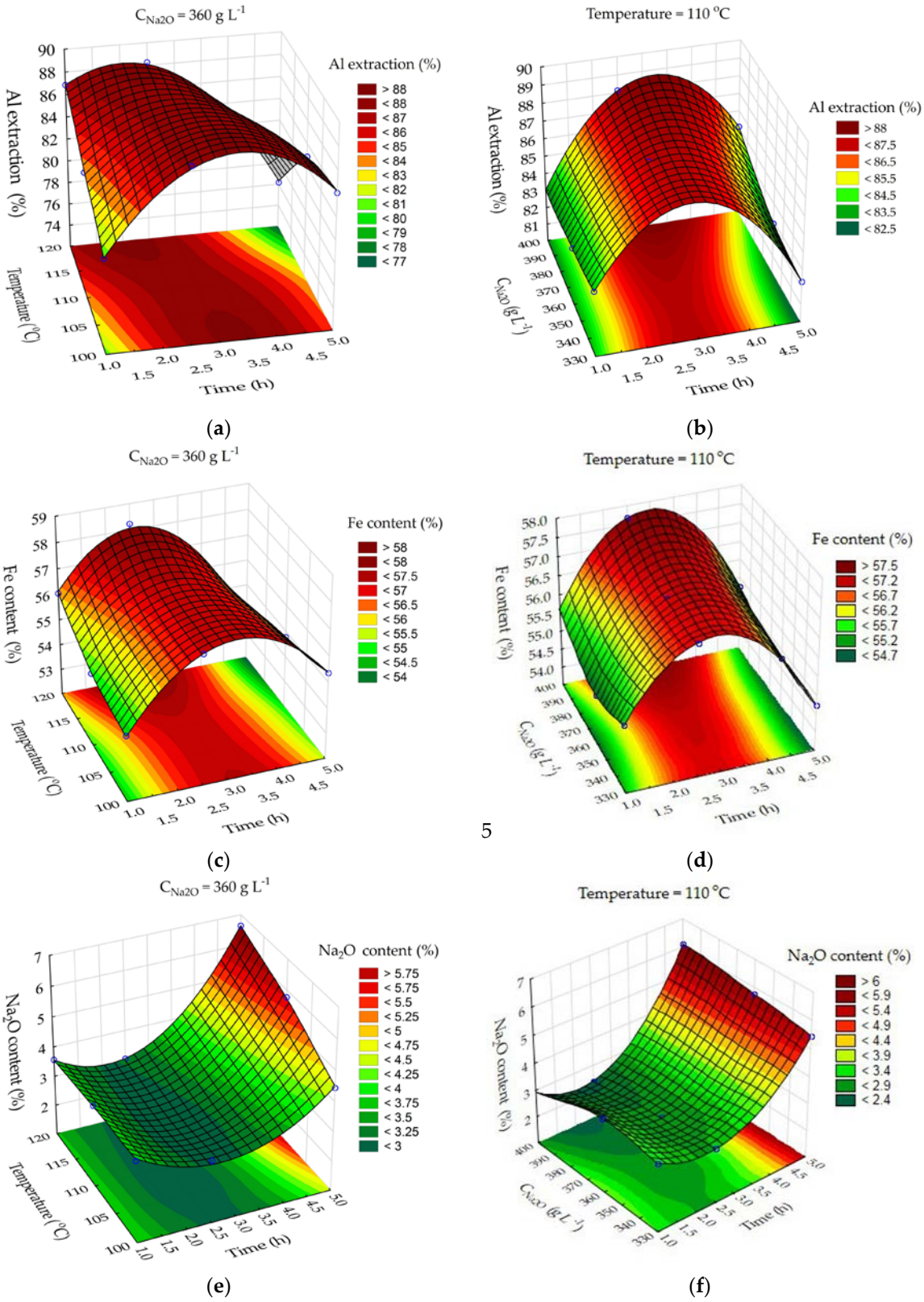


**Figure 6.** Neural network response surfaces for effect of time and temperature on the Al extraction from bauxite residue (BR) (a); effect of time and $Na_2O$ concentration on the Al extraction from BR (b); effect of time and temperature on the Fe content in the solid residue (c); effect of time and $Na_2O$ concentration on the Fe content in the solid residue (d); effect of time and temperature on the $Na_2O$ content in the solid residue (e); effect of time and $Na_2O$ concentration on the $Na_2O$ content in the solid residue (f).

According to Figure 6a, the major effect on Al extraction is caused by leaching time. After 2 h of leaching at T = 120 °C and $C_{Na2O}$ 360 g $L^{-1}$, the Al extraction degree was > 95%.

Preprints (www.preprints.org) | NOT PEER-REVIEWED | Posted: 7 November 2022 doi:10.20944/preprints202211.0105.v1

After 2-2.5 h of leaching, the solid residue has the highest Fe content (Figure 7b). Therefore, the optimal leaching parameters for Sands and BR can be as follows: T = 120 °C, $C_{Na2O}$ = 360 g $L^{-1}$, and leaching time = 2.5 h. The content of Fe in the sands solid residue at these conditions was about 70%, while the $Na_2O$ content was less than 0.25% (Figure 7c) and this product can be used as a pigment-quality magnetite.

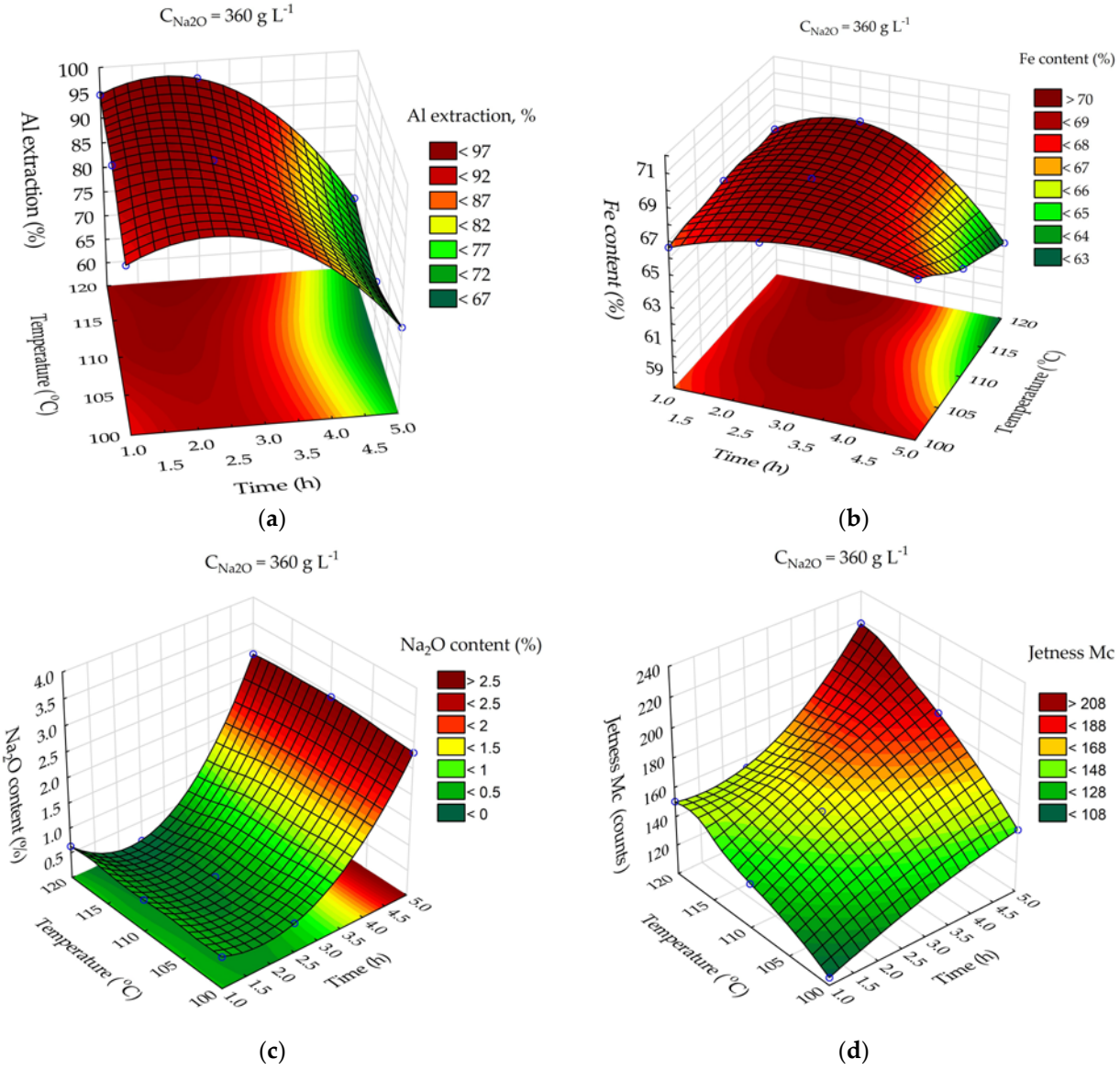


**Figure 7.** Neural network response surfaces for effect of time and temperature on the Al extraction from sands (a); effect of time and temperature on the Fe content in the sands residue (b); effect of time and temperature on the $Na_2O$ content in the sands residue (c); effect of time and temperature on the jetness (d).

One of the most important characteristics of the pigments is their jetness. Figure 7d illustrates how leaching time and temperature affect the jetness of the magnetite concentrate obtained after the leaching of sands in the presence of $Fe^{2+}$. According to this data, 5 h of leaching is necessary to achieve a jetness higher than 200. It should be noted, that the jetness of modern pigments can be higher than 300 [43]. Therefore, there is a dilemma in achieving both high jetness and low impurities amounts, because after 5 h of leaching, the $Na_2O$ content increases to 2.5%.

One of the possible solutions to this problem is double leaching, in which Al and Si are removed with a partial transfer of goethite to magnetite at the 1st stage, and the product

 doi:10.20944/preprints202211.0105.v1

is then subjected to a 'curing process' in a pure alkaline solution to obtain the required degree of blackness at the second stage.

*3.2. Leaching kinetics*

During a fluid-particle heterogenous reaction a solid particle reacts with a liquid with the formation of a solid product. If the solid particle that reacts with a liquid shrinks in size then a shrinking core model can be used to describe this process [44]. According to the model, the reaction has five steps: diffusion through the liquid film, diffusion through the product layer, the surface chemical reaction, liquid or gas product diffusion through the product layer, and product diffusion through the liquid film to the solution. The slowest step of this process is referred to as the rate limiting step. There are three main models of a shrinking core that used to describe the process: Equation (13), which describes diffusion through the liquid film, Equation (14), which describes diffusion through the product layer, and Equation (15), which describes reaction on the surface of the core.

$$X = kt, \quad (13)$$

$$1 - 3(1 - X)^{2/3} + 2(1 - X) = kt, \quad (14)$$

$$1 - (1 - X)^{1/3} = kt. \quad (15)$$

These equations are valid for the leaching of a solid with a uniform particle size distribution [44]. Therefore, Equations (13)-(15) were used to describe the extraction fraction of Al (X) from the different minerals of the raw sands (Figure 8a-8c). Only 2 h leaching time was used in the kinetics calculation because after this time the fresh DSP began to precipitate (Figure 6). The gibbsite that was not leached during the Bayer process and the Al that can be included in the Al-goethite were denoted as a "solid matrix" and the Al that contained in the DSP was denoted as a "DSP". The results of fitting the experimental data in Equations (12)-(14) are shown in Table 4, where the correlation coefficient values ($R^2$) and the corresponding leaching rate constants (k) for all plots in Figure 8a-8c are listed. The intraparticle diffusion model (Equation (13)) showed the highest convergence with the extraction of Al from the DSP. Because the DSP has a low leaching efficiency, it can be assumed that the product layer consists of silica-containing minerals that are insoluble at these leaching conditions.

During “Solid matrix” phase leaching, there is no new solid product, but the solid matrix of iron minerals that includes Al-goethite can play a role of a reaction solid product. However, the model of the surface chemical reaction (Equation 14) was best to fit the data of Al extraction from the "solid matrix" phase. The Arrhenius plots of lnk versus 1000/T were constructed after the rate constants for both processes were calculated. The activation energy for Al extraction from "DSP" phase was 30.9 kJ/mol, and for Al extraction from "solid matrix" phase it was 36.7 kJ/mol. The activation energy greater than 40 kJ/mol is typical for a leaching process limited by the surface reaction [45]. Therefore, it confirms that the extraction of Al from a "solid matrix" phase is more temperature dependent and can be limited by the surface reaction.

Figure 8 shows that the Al extraction degree from the solid matrix of iron containing minerals is high (almost 100 %) using leaching with the transformation of goethite (hematite) to magnetite. This can be explained by the fact that goethite should be dissolved before a new solid phase (magnetite) can form [46]. The Al extraction degree from DSP is relatively low because sodalite is insoluble in the alkaline media until a new phase is formed, for example hydrogarnet [47]. Moreover, after the concentration of silicon in the solution reaches a certain value, the DSP begins to precipitate again (Figure 6). To enhance the Al extraction degree from DSP, it is necessary to use several leaching cycles or add lime.

Preprints (www.preprints.org) | NOT PEER-REVIEWED | Posted: 7 November 2022 doi:10.20944/preprints202211.0105.v1

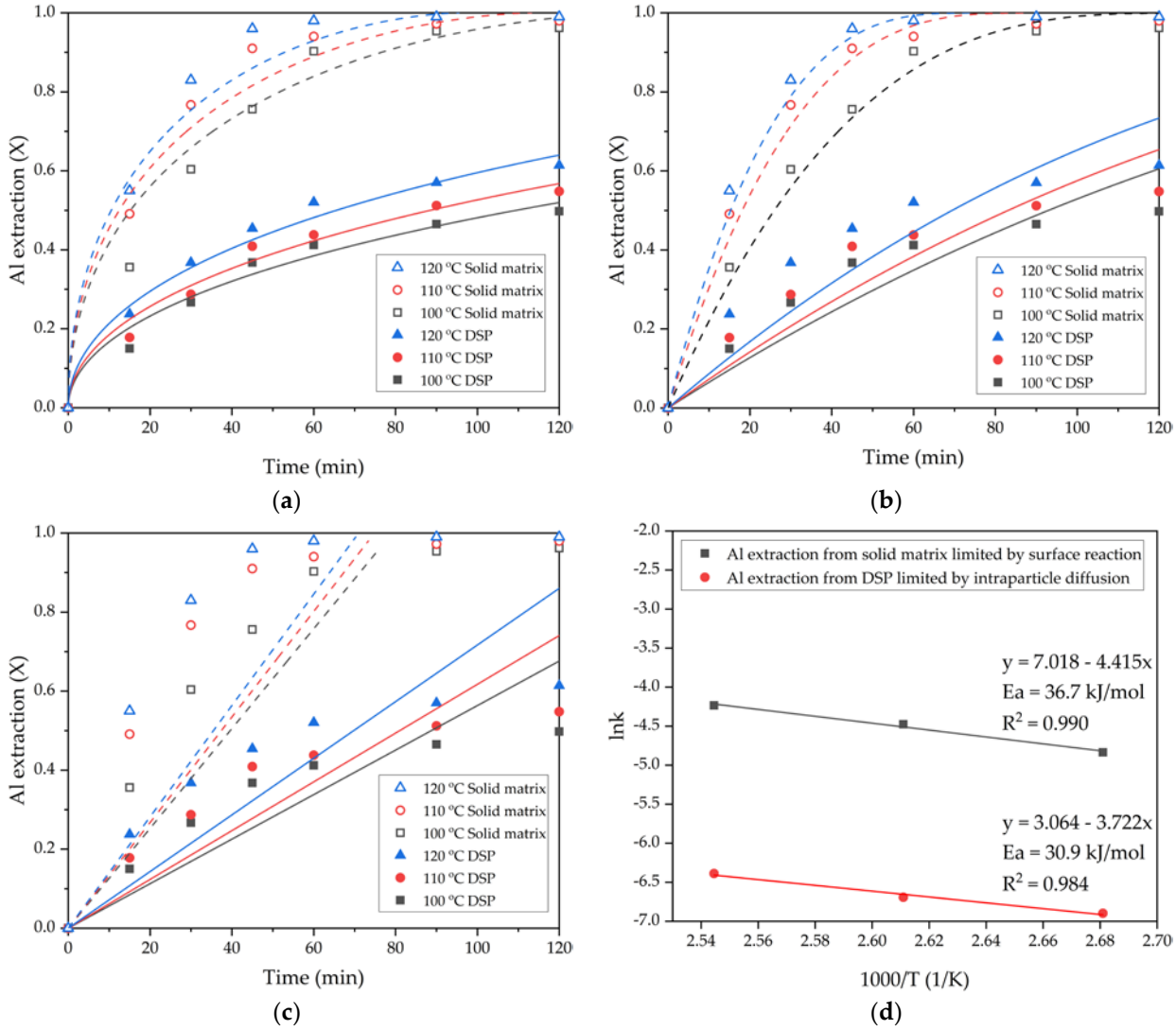


**Figure 8.** The results of fitting the obtained data for the effect of temperature on the Al extraction from the different phases (points) to Equations (12)-(14) (lines): the diffusion through the product layer (a); the surface chemical reaction (b); the diffusion through the liquid film (c); the apparent rate constants of the Al extraction from the different phases at different temperatures plotted vs. the inverse temperature (Arrhenius plots) (d).

**Table 4.** The results of the experimental data (figure 7) fitting to the shrinking core models.

| Equation | Al containing phase | Temperature, °C | Apparent rate constant k ($min^{-1}$) | $R^2$ (%) |
|---|---|---|---|---|
| Diffusion through the product layer (Figure 7a) | DSP | 100 | 0.0010 | 0.964 |
| | | 110 | 0.0012 | 0.972 |
| | | 120 | 0.0017 | 0.967 |
| | Solid matrix | 100 | 0.0076 | 0.904 |
| | | 110 | 0.0088 | 0.865 |
| | | 120 | 0.0105 | 0.800 |
| Surface chemical reaction (Figure 7b) | DSP | 100 | 0.0022 | 0.851 |
| | | 110 | 0.0025 | 0.861 |
| | | 120 | 0.0030 | 0.830 |
| | Solid matrix | 100 | 0.0079 | 0.996 |
| | | 110 | 0.0114 | 0.966 |
| | | 120 | 0.0145 | 0.971 |

Preprints (www.preprints.org) | NOT PEER-REVIEWED | Posted: 7 November 2022 doi:10.20944/preprints202211.0105.v1

| | | | | |
|---|---|---|---|---|
| Diffusion through the liquid film (Figure 7c) | DSP | 100 | 0.0044 | 0.929 |
| | | 110 | 0.0048 | 0.930 |
| | | 120 | 0.0055 | 0.912 |
| | Solid matrix | 100 | 0.0090 | 0.870 |
| | | 110 | 0.0093 | 0.852 |
| | | 120 | 0.0095 | 0.832 |

*3.3. Solid residues characterisation*

3.3.1. Chemical composition of the residues

After 2.5 h of leaching at a ferrous sulfate to bauxite residue ratio of 1:1 and 120 °C in alkaline media, the alumina extraction ratio is 96.27% for Sand and 87.06% for BR. At these conditions, the Fe content in the sands residue and in the BRresidues can be increased to 69.55% and 58.31%, respectively. Table 5 shows the chemical compositions of the solid residues obtained after BR and Sands leaching at optimal parameters.

**Table 5.** The chemical compositions of the solid residues obtained after leaching, wt. % (T = 120 °C, τ = 2.5 h, $FeSO_4$ to BR ratio of 1:1).

| Sample | Fe | Si | Ti | Al | Na | O | Sc | P | S | Other |
|---|---|---|---|---|---|---|---|---|---|---|
| BR solid residue | 58.31 | 2.06 | 3.92 | 1.33 | 1.45 | 31.35 | 0.006 | 0.007 | 0.08 | 1.58 |
| Sands solid residue | 69.55 | 0.34 | 1.01 | 0.15 | 0.24 | 27.81 | 0.005 | 0.009 | 0.003 | 0.90 |

Table 5 shows that the solid residue from leaching of sands contains low amounts of impurities: Na and Al are less than 0.25%. The content of Si and Ti in this residue is also smaller than in traditional bauxite residues. The higher contents of Na, Ti, Si and Al in the solid residue obtained after BR leaching makes it difficult to use this product as a pigment. The high Na content will also hinder its use for iron production. Therefore, preliminary leaching with acid or lime causticisation should be used to further improve the valorization of the BR residues. The P and S content in these products is lower than 0.1% (Table 5), which would be beneficial for iron production.

To evaluate why there is such a difference in the results obtained using BR and Sands, the XRD patterns (Figure 3) of the solid residues were investigated. The higher amount of hematite (Al-hematite) in BR (Figure 3) results in the incompleteness of the process (the formation of magnetite from goethite is a faster process from a thermodynamic viewpoint) [48]. Furthermore, there is a higher amount of sodalite (DSP) in BR that will not fully dissolve in the alkaline media without lime addition, which leads to the higher Na content in the residue. From the XRD patterns, it can be confirmed that the conversion of goethite and hematite to magnetite is more effective for sands. To support this hypothesis, a SEM-EDX and the Mössbauer analysis of the solid residue was conducted.

According to elemental mapping of the solid residues (Figure 9a and 9b), it is obvious that the BR solid residue has high amount of Al, Si and lesser amount of Fe. This confirms previous observations. Furthermore, the particle size of the Sands residue is smaller (see Figures 9c and 9d), and there can be seen particles of the raw BR in Figure 9e.

Preprints (www.preprints.org) | NOT PEER-REVIEWED | Posted: 7 November 2022 doi:10.20944/preprints202211.0105.v1

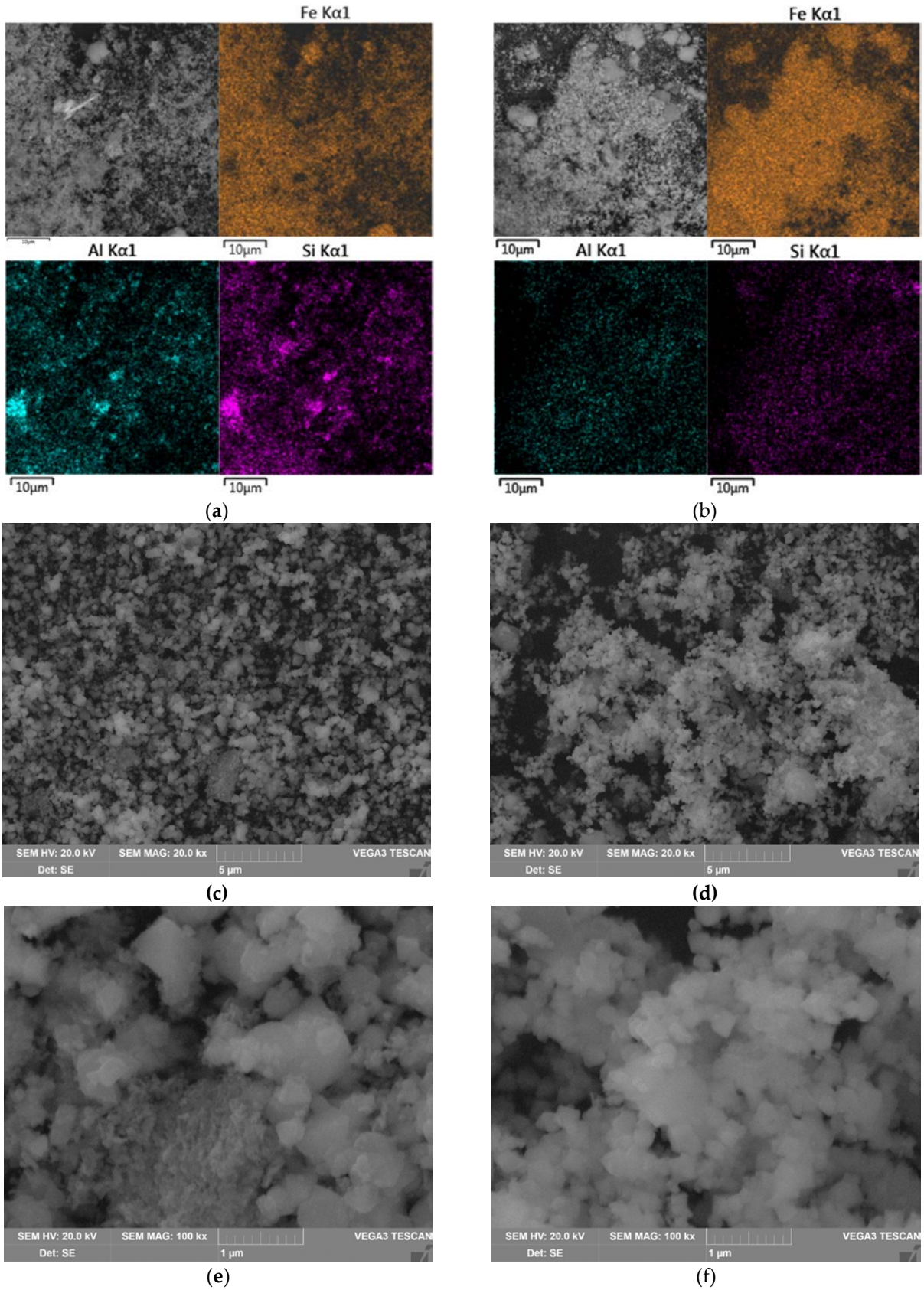


**Figure 9.** Mapping and morphology of BR and Sands residue surface using SEM-EDX analysis: BSE image and mapping of the BR residue surface (a); BSE image and mapping of the Sands residue surface (b); SEM image of the BR residue surface at 20 kx magnitude (c); SEM image of the Sands residue surface at 20 kx magnitude (d); SEM image of the BR residue surface at 100 kx magnitude (e); SEM image of the Sands residue surface at 100 kx magnitude (f).

Preprints (www.preprints.org) | NOT PEER-REVIEWED | Posted: 7 November 2022 doi:10.20944/preprints202211.0105.v1

3.3.2. Mössbauer analysis

At room temperature, the Mössbauer spectra of the BR and Sands residue samples contain six asymmetric lines of different widths and intensities, some of which split into two in the region of negative velocities (Figure 10). At the same time, significant extended absorption is observed in the central part of the spectrum of the BR residue sample. When the samples are cooled to the boiling point of nitrogen, the lines usually narrow, but their splitting and the presence of shoulders indicate that the iron atoms have several crystallographic positions that differ significantly from each other. Indeed, experimental spectra can only be satisfactorily described using at least four symmetrical sextets (and one doublet for high-temperature spectra) (Table 6).

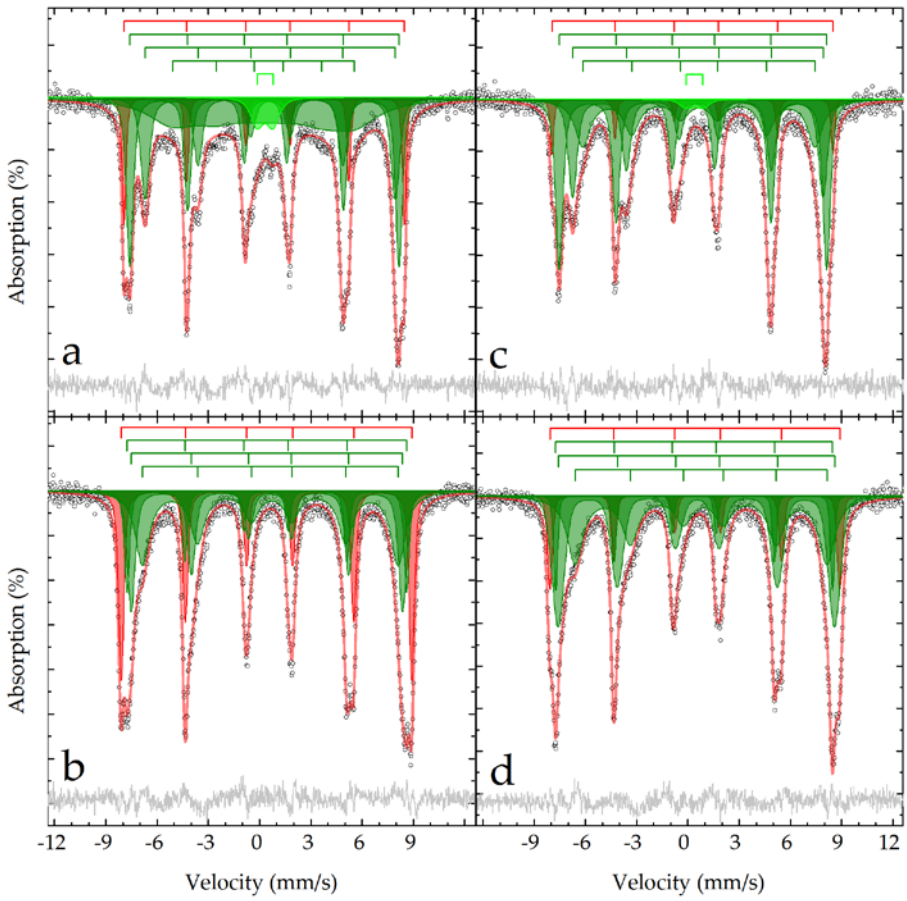


**Figure 10.** Mössbauer spectra obtained at 296 K (a, c) and 77.6 K (b, d) of the BR residue (a, b) and Sands residue (c, d) samples and their model description according to Table 6.

The outer sextet with rather narrow lines belongs to the Al-hematite described above for the raw materials. Moreover, if for the raw materials the proportion of Al-hematite in the BR sample was almost one and a half times higher (Table 2), then after treatment the proportion of Al-hematite in the BR residue sample is two times higher compared to the Sands residue sample (Table 6). Similarly, to the procedure described above, using equation (12), one can estimate the compositions of Al-hematite as $\alpha$-$(Fe_{0.96}Al_{0.04})_2O_3$ and $\alpha$-$(Fe_{0.94}Al_{0.06})_2O_3$ in the corresponding samples.

The remaining three sextets correspond to iron atoms in different crystallographic positions for nonstoichiometric magnetite of the composition $Fe_{3-\delta}O_4 \equiv (Fe^{3+})_A(Fe^{2+}{}_{1-3\delta}Fe^{3+}{}_{1+2\delta}\#_\delta)_BO_4$ [49,50]. By analyzing the areas and isomeric shifts of the subspectra related to iron atoms in different crystallographic sites of magnetite, it is possible to estimate the value of the magnetite nonstoichiometric parameter - δ, using the Equation (16) [51]:

$$\delta = \{\Sigma(\delta_2-3\delta_i+2\delta_3)*S_i + (\delta_2-\delta_3)\Sigma S_j\}/\{\Sigma(3\delta_2-\delta_i-2\delta_3)*S_i + 3(\delta_2-\delta_3)\Sigma S_j\}, \quad (16)$$

Preprints (www.preprints.org) | NOT PEER-REVIEWED | Posted: 7 November 2022 doi:10.20944/preprints202211.0105.v1

where $S_i$ is the relative area of the subspectrum with isomeric shift $\delta_i$ related to iron atoms in the B-site, $S_j$ is the relative area of the remaining subspectra, $\delta_2$ and $\delta_3$ are isomeric shifts of iron atoms (+2) and (+3) in an octahedral oxygen environment for a given temperature (here $\delta_2$ = 1.16±0.06 and 1.33±0.09 mm/s for 296 and 78 K, respectively, and $\delta_3$ = 0.37±0.04 and 0.49±0.04 mm/s for 296 and 78 K, respectively [41]). The results obtained for different temperatures are in good agreement with each other and make it possible to describe the composition of the samples as $Fe_{2.75}O_4$ and $Fe_{2.85}O_4$ for BR residue and Sands residue, respectively, so the first sample is more oxidized.

The hyperfine parameters of the minor doublet observed only at room temperature correspond to $Fe^{3+}$ ions in an octahedral oxygen environment [41].

**Table 6.** The subspectrum parameters describing experimental Mössbauer spectra obtained at different temperatures for BR residue and Sands residue samples.

| Sample | | | BR residue | | | | | | Sands residue | | | | | |
|---|---|---|---|---|---|---|---|---|---|---|---|---|---|---|
| Temperature, K | Phase | № | δ | ε (Δ=2ε) | $\Gamma_{exp}$ | $H_{eff}$ | S | δ in $Fe_{3-\delta}O_4$ | δ | ε (Δ=2ε) | $\Gamma_{exp}$ | $H_{eff}$ | S | δ in $Fe_{3-\delta}O_4$ |
| | | | mm/s | | | kOe | % | | mm/s | | | kOe | % | |
| 296 | $\alpha$-$(Fe_{1-x}Al_x)_2O_3$ | 1 | 0.38±0.01 | -0.10±0.01 | 0.28±0.01 | 508.7±0.2 | 12.4±0.6 | | 0.38±0.01 | -0.11±0.01 | 0.24±0.01 | 509.8±0.3 | 6.1±0.4 | |
| | $Fe_{3-\delta}O_4$ | 2 | 0.32±0.01 | -0.03±0.01 | 0.49±0.01 | 488.4±0.2 | 29±1 | | 0.32±0.01 | -0.02±0.01 | 0.52±0.01 | 485.3±0.2 | 40.3±0.8 | |
| | | 3 | 0.63±0.01 | -0.01±0.01 | 0.62±0.01 | 454.0±0.2 | 22.4±0.7 | 0.15 | 0.62±0.01 | -0.03±0.01 | 0.61±0.02 | 454.4±0.4 | 27±2 | 0.25 |
| | | 4 | 0.38±0.01 | -0.16±0.03 | 3.5±0.2 | 330±4 | 32±2 | | 0.65±0.01 | -0.00±0.01 | 1.06±0.04 | 422±2 | 25±2 | |
| | $Fe^{3+}_{Oh}$ | 5 | 0.32±0.02 | (0.94±0.03) | 0.89±0.07 | | 4.3±0.3 | | 0.38±0.01 | (0.94±0.01) | 0.9±0.2 | | 1.6±0.2 | |
| 77.6 | $\alpha$-$(Fe_{1-x}Al_x)_2O_3$ | 1 | 0.50±0.01 | -0.09±0.01 | 0.37±0.01 | 527.3±0.2 | 27.4±0.8 | | 0.49±0.01 | -0.08±0.01 | 0.36±0.01 | 526.0±0.3 | 12.6±0.9 | |
| | $Fe_{3-\delta}O_4$ | 2 | 0.40±0.01 | 0.03±0.01 | 0.37±0.01 | 507.7±0.4 | 15±1 | | 0.37±0.01 | -0.01±0.01 | 0.30±0.01 | 502.6±0.2 | 10.5±0.8 | |
| | | 3 | 0.52±0.01 | -0.09±0.01 | 0.55±0.02 | 492.5±0.5 | 26±2 | 0.16 | 0.52±0.01 | -0.03±0.01 | 0.87±0.02 | 501.6±0.7 | 42±1 | 0.24 |
| | | 4 | 0.67±0.01 | -0.04±0.01 | 1.00±0.03 | 464.2±0.8 | 32±1 | | 0.84±0.01 | -0.07±0.01 | 1.12±0.03 | 457.2±0.9 | 35±1 | |

$\delta$ – Isomer shift; ε (Δ) - Quadrupole shift (splitting); $\Gamma_{exp}$ – Line width; $H_{eff}$ – Hyperfine magnetic field; $S$ – Relative area of a subspectrum №, "δ in $Fe_{3-\delta}O_4$" - magnetite nonstoichiometric parameter [51].

### 3.3.3. Magnetization

Figure 10 shows the magnetization measurements of the samples. Both raw samples appear to be magnetically inert. The residues magnetization reaches a saturation value (Ms) of 45–60 emu $g^{-1}$ at a magnetic field of 10 kOe. These values are lower than those of pure synthetic magnetite according to the literature (70-90 emu $g^{-1}$) [55]. However, the values are comparable with those determined for magnetite concentrates obtained from BRs [25]. As shown in Figure 10, the magnetization of both the BR residue and sand residue increases with increasing leaching duration. Also, the Ms of the BR residues is lower at all leaching durations. This can be explained by the higher level of impurities in the case of the BR residues.

Preprints (www.preprints.org) | NOT PEER-REVIEWED | Posted: 7 November 2022 doi:10.20944/preprints202211.0105.v1

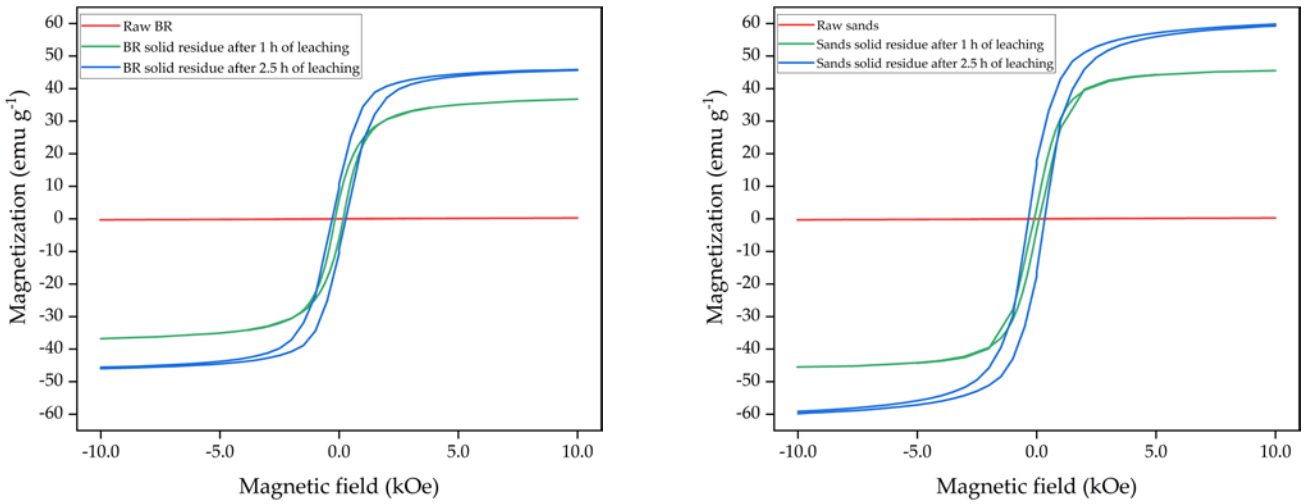


(**a**) (**b**)

**Figure 10.** Magnetization curves for the BR and the BR solid residues obtained after BR leaching at 110 °C, $C_{Na2O}$ 360 g $L^{-1}$ during 1h and 2.5 h (a); the sands and the sands solid residues obtained after BR leaching at 110 °C, $C_{Na2O}$ 360 g $L^{-1}$ during 1h and 2.5 h (b).

## 4. Conclusions

In this study, the novel method of treating high-iron bauxite residues from the Friguia alumina refinery using low-temperature leaching in the presence of $Fe^{2+}$ was investigated.

According to the XRD, TG-DTA and Mössbauer analysis, aluminum in this type of BR is presented by Al-hematite and Al-goethite, that are insoluble in the common Bayer leaching. The leaching in the presence of $Fe^{2+}$ accelerates Al extraction from Al-hematite and Al-goethite. This effect is caused by the magnetization of magnetite and goethite after they are dissolved in a concentrated alkaline solution. The analysis of the Al extraction degree, Fe and $Na_2O$ content in residue obtained by alkaline leaching in the presence of $Fe^{2+}$ was performed using ANNs and machine learning. The optimal leaching parameters were found to be T = 120 °C, L:S = 10, and τ = 2.5 h, $C_{Na2O}$ = 360 g $L^{-1}$. At these parameters, the alumina extraction degree reached 96.27% for sand and 86.07% for bauxite residue. The grade of iron (total iron in the form of iron element) in the residue can be increased to 69.55% for Sands and 58.31% for BR.

The extremely low impurities content in the solid residue obtained after the Sands leaching and the high blackness make it a good alternative for pigment production. The difference in extraction degree and total Fe content in the solid residues obtained from Sands and BR can be attributed to the higher amount of Al-hematite and sodalite in BR. Sc acid leaching or lime causticization can be used to reduce the amount of sodalite in BR before it is valorized.

**Author Contributions:** Conceptualization, A.S. and I.L.; methodology, M.M.D.; software, D.V.; validation, D.V. and D.P.; formal analysis, Y.O.; investigation, A.R. and M.M.D.; resources, M.C.B.; data curation, M.C.B.; writing—original draft preparation, A.S. and A.R.; writing—review and editing, D.V. and D.P.; visualization, Y.O. and A.S.; supervision, D.P.; project administration, I.L.; funding acquisition, I.L. All authors have read and agreed to the published version of the manuscript.

**Funding:** This research was funded by RSCF, grant number 22-29-01515.

The SEM-EDS, VSM and XRD analysis was funded by the Project of the State Assignment, FEUZ-2021-0017. The methods for determining the chemical composition of BR, sands and leaching residues by XRF and ICP-MS (see Section 2.3. "Chemical composition of samples") were funded by the Project of the State Assignment (Vernadsky Institute of Geochemistry and Analytical Chemistry of Russian Academy of Sciences, № FMUS-2019-24). Mössbauer analysis was performed in accordance with the state assignment of Lomonosov Moscow State University "Solving of problems

of nuclear energy and environmental safety problems, as well as diagnostics of materials using ionizing radiation" (Project Reg. No. 122030200324-1).

**Institutional Review Board Statement:** Not applicable.

**Informed Consent Statement:** Not applicable.
**Data Availability Statement:** Not applicable.

**Acknowledgments:** The authors express our gratitude to Evgeny Kolesnikov from NUST MISiS for assistance of the SEM-EDX, and XRD analyses of solid samples.

**Conflicts of Interest:** The authors declare no conflict of interest.

## References

1. Swain, B.; Akcil, A.; Lee, J. Red Mud Valorization an Industrial Waste Circular Economy Challenge; Review over Processes and Their Chemistry. *Crit. Rev. Environ. Sci. Technol.* **2022**, *52*, 520–570, doi:10.1080/10643389.2020.1829898.
2. Cui, Y.; Chen, J.; Zhang, Y.; Peng, D.; Huang, T.; Sun, C. PH-Dependent Leaching Characteristics of Major and Toxic Elements from Red Mud. *Int. J. Environ. Res. Public. Health* **2019**, *16*, 2046, doi:10.3390/ijerph16112046.
3. Ruyters, S.; Mertens, J.; Vassilieva, E.; Dehandschutter, B.; Poffijn, A.; Smolders, E. The Red Mud Accident in Ajka (Hungary): Plant Toxicity and Trace Metal Bioavailability in Red Mud Contaminated Soil. *Environ. Sci. Technol.* **2011**, *45*, 1616–1622, doi:10.1021/es104000m.
4. Winkler, D.; Bidló, A.; Bolodár-Varga, B.; Erdő, Á.; Horváth, A. Long-Term Ecological Effects of the Red Mud Disaster in Hungary: Regeneration of Red Mud Flooded Areas in a Contaminated Industrial Region. *Sci. Total Environ.* **2018**, *644*, 1292–1303, doi:10.1016/j.scitotenv.2018.07.059.
5. Liu, Z.; Li, H. Metallurgical Process for Valuable Elements Recovery from Red Mud—A Review. *Hydrometallurgy* **2015**, *155*, 29–43, doi:10.1016/j.hydromet.2015.03.018.
6. Liu, Y.; Naidu, R. Hidden Values in Bauxite Residue (Red Mud): Recovery of Metals. *Waste Manag.* **2014**, *34*, 2662–2673, doi:10.1016/j.wasman.2014.09.003.
7. Loginova, I.V.; Shoppert, A.A.; Chaikin, L.I. Extraction of Rare-Earth Metals During the Systematic Processing of Diaspore-Boehmite Bauxites. *Metallurgist* **2016**, *60*, 198–203, doi:10.1007/s11015-016-0273-z.
8. Shiryaeva, E.V.; Podgorodetskii, G.S.; Malysheva, T.Ya.; Gorbunov, V.B.; Zavodyanyi, A.V.; Shapovalov, A.N. Effects of Adding Low-Alkali Red Mud to the Sintering Batch at OAO Ural'skaya Stal'. *Steel Transl.* **2014**, *44*, 6–10, doi:10.3103/S0967091214010173.
9. Loginova, I.V.; Shoppert, A.A.; Chaikin, L.I. Effect of Adding Sintering Furnace Electrostatic Precipitator Dust on Combined Leaching of Bauxites and Cakes. *Metallurgist* **2015**, *59*, 698–704, doi:10.1007/s11015-015-0161-y.
10. Alkan, G.; Yagmurlu, B.; Gronen, L.; Dittrich, C.; Ma, Y.; Stopic, S.; Friedrich, B. Selective Silica Gel Free Scandium Extraction from Iron-Depleted Red Mud Slags by Dry Digestion. *Hydrometallurgy* **2019**, *185*, 266–272, doi:10.1016/j.hydromet.2019.03.008.
11. Shoppert, A.; Loginova, I.; Napol'skikh, J.; Valeev, D. High-Selective Extraction of Scandium (Sc) from Bauxite Residue (Red Mud) by Acid Leaching with MgSO4. *Materials* **2022**, *15*, 1343, doi:10.3390/ma15041343.
12. Shoppert, A.; Loginova, I.; Napol'skikh, J.; Kyrchikov, A.; Chaikin, L.; Rogozhnikov, D.; Valeev, D. Selective Scandium (Sc) Extraction from Bauxite Residue (Red Mud) Obtained by Alkali Fusion-Leaching Method. *Materials* **2022**, *15*, 433, doi:10.3390/ma15020433.
13. Huang, Y.; Chai, W.; Han, G.; Wang, W.; Yang, S.; Liu, J. A Perspective of Stepwise Utilisation of Bayer Red Mud: Step Two—Extracting and Recovering Ti from Ti-Enriched Tailing with Acid Leaching and Precipitate Flotation. *J. Hazard. Mater.* **2016**, *307*, 318–327, doi:10.1016/j.jhazmat.2016.01.010.
14. Pasechnik, L.A.; Skachkov, V.M.; Chufarov, A.Yu.; Suntsov, A.Yu.; Yatsenko, S.P. High Purity Scandium Extraction from Red Mud by Novel Simple Technology. *Hydrometallurgy* **2021**, *202*, 105597, doi:10.1016/j.hydromet.2021.105597.

15. Beavogui, M.C.; Balmaev, B.G. Influence of grain-size composition of bauxite on its recovery at Fria aluminum plant in Guinea. *Min. Informational Anal. Bull.* **2017**, *9*, 131–138, doi:10.25018/0236-1493-2017-9-0-131-138.
16. Valeev, D.; Pankratov, D.; Shoppert, A.; Sokolov, A.; Kasikov, A.; Mikhailova, A.; Salazar-Concha, C.; Rodionov, I. Mechanism and Kinetics of Iron Extraction from High Silica Boehmite–Kaolinite Bauxite by Hydrochloric Acid Leaching. *Trans. Nonferrous Met. Soc. China* **2021**, *31*, 3128–3149, doi:10.1016/S1003-6326(21)65721-7.
17. Li, G.; Liu, M.; Rao, M.; Jiang, T.; Zhuang, J.; Zhang, Y. Stepwise Extraction of Valuable Components from Red Mud Based on Reductive Roasting with Sodium Salts. *J. Hazard. Mater.* **2014**, *280*, 774–780, doi:10.1016/j.jhazmat.2014.09.005.
18. Alkan, G.; Schier, C.; Gronen, L.; Stopic, S.; Friedrich, B. A Mineralogical Assessment on Residues after Acidic Leaching of Bauxite Residue (Red Mud) for Titanium Recovery. *Metals* **2017**, *7*, 458, doi:10.3390/met7110458.
19. Cardenia, C.; Balomenos, E.; Wai Yin Tam, P.; Panias, D. A Combined Soda Sintering and Microwave Reductive Roasting Process of Bauxite Residue for Iron Recovery. *Minerals* **2021**, *11*, 222, doi:10.3390/min11020222.
20. Anawati, J.; Azimi, G. Integrated Carbothermic Smelting – Acid Baking – Water Leaching Process for Extraction of Scandium, Aluminum, and Iron from Bauxite Residue. *J. Clean. Prod.* **2022**, *330*, 129905, doi:10.1016/j.jclepro.2021.129905.
21. Zhang, Y.; Lü, W.; Qi, Y.; Zou, Z. Recovery of Iron and Calcium Aluminate Slag from High-Ferrous Bauxite by High-Temperature Reduction and Smelting Process. *Int. J. Miner. Metall. Mater.* **2016**, *23*, 881–890, doi:10.1007/s12613-016-1303-3.
22. Valeev, D.; Zinoveev, D.; Kondratiev, A.; Lubyanoi, D.; Pankratov, D. Reductive Smelting of Neutralized Red Mud for Iron Recovery and Produced Pig Iron for Heat-Resistant Castings. *Metals* **2019**, *10*, 32, doi:10.3390/met10010032.
23. Li, X.; Wang, Y.; Zhou, Q.; Qi, T.; Liu, G.; Peng, Z.; Wang, H. Transformation of Hematite in Diasporic Bauxite during Reductive Bayer Digestion and Recovery of Iron. *Trans. Nonferrous Met. Soc. China* **2017**, *27*, 2715–2726, doi:10.1016/S1003-6326(17)60300-5.
24. Li, X.; Yu, S.; Dong, W.; Chen, Y.; Zhou, Q.; Qi, T.; Liu, G.; Peng, Z.; Jiang, Y. Investigating the Effect of Ferrous Ion on the Digestion of Diasporic Bauxite in the Bayer Process. *Hydrometallurgy* **2015**, *152*, 183–189, doi:10.1016/j.hydromet.2015.01.001.
25. Pasechnik, L.A.; Skachkov, V.M.; Bogdanova, E.A.; Chufarov, A.Y.; Kellerman, D.G.; Medyankina, I.S.; Yatsenko, S.P. A Promising Process for Transformation of Hematite to Magnetite with Simultaneous Dissolution of Alumina from Red Mud in Alkaline Medium. *Hydrometallurgy* **2020**, *196*, 105438, doi:10.1016/j.hydromet.2020.105438.
26. Zhou, G.; Wang, Y.; Qi, T.; Zhou, Q.; Liu, G.; Peng, Z.; Li, X. Cleaning Disposal of High-Iron Bauxite Residue Using Hydrothermal Hydrogen Reduction. *Bull. Environ. Contam. Toxicol.* **2022**, *109*, 163–168, doi:10.1007/s00128-022-03516-4.
27. Vu, H.; Jandová, J.; Hron, T. Recovery of Pigment-Quality Magnetite from Jarosite Precipitates. *Hydrometallurgy* **2010**, *101*, 1–6, doi:10.1016/j.hydromet.2009.10.007.
28. Boháček, J.; Šubrt, J.; Hanslík, T.; Tláskal, J. Preparing Particulate Magnetites with Pigment Properties from Suspensions of Basic Iron(III) Sulphates with the Structure of Jarosite. *J. Mater. Sci.* **1993**, *28*, 2827–2832, doi:10.1007/BF00356226.
29. Hage, J.L.T.; Schuiling, R.D.; Vriend, S.P. Production of Magnetite from Sodiumjarosite Under Reducing Hydrothermal Conditions. The Reduction of $Fe^{III}$ to $Fe^{II}$ with Cellulose. *Can. Metall. Q.* **1999**, *38*, 267–276, doi:10.1179/cmq.1999.38.4.267.
30. Zhou, G.; Wang, Y.; Qi, T.; Zhou, Q.; Liu, G.; Peng, Z.; Li, X. Comprehensive Utilization of Al-Goethite-Containing Red Mud Treated Through Low-Temperature Sodium Salt-Assisted Roasting–Water Leaching. *J. Sustain. Metall.* **2022**, *8*, 825–836, doi:10.1007/s40831-022-00538-4.
31. Ingram-Jones, V.J.; Slade, R.C.T.; Davies, T.W.; Southern, J.C.; Salvador, S. Dehydroxylation Sequences of Gibbsite and Boehmite: Study of Differences between Soak and Flash Calcination and of Particle-Size Effects. *J. Mater. Chem.* **1996**, *6*, 73, doi:10.1039/jm9960600073.
32. Derie, R.; Ghodsi, M.; Calvo-Roche, C. DTA Study of the Dehydration of Synthetic Goethite AFeOOH. *J. Therm. Anal.* **1976**, *9*, 435–440, doi:10.1007/BF01909409.

33. Marsh, A.; Heath, A.; Patureau, P.; Evernden, M.; Walker, P. A Mild Conditions Synthesis Route to Produce Hydrosodalite from Kaolinite, Compatible with Extrusion Processing. *Microporous Mesoporous Mater.* **2018**, *264*, 125–132, doi:10.1016/j.micromeso.2018.01.014.
34. Grudinsky, P.; Zinoveev, D.; Pankratov, D.; Semenov, A.; Panova, M.; Kondratiev, A.; Zakunov, A.; Dyubanov, V.; Petelin, A. Influence of Sodium Sulfate Addition on Iron Grain Growth during Carbothermic Roasting of Red Mud Samples with Different Basicity. *Metals* **2020**, *10*, 1571, doi:10.3390/met10121571.
35. Rostovshchikova, T.N.; Smirnov, V.V.; Tsodikov, M.V.; Bukhtenko, O.V.; Maksimov, Yu.V.; Kiseleva, O.I.; Pankratov, D.A. Catalytic Conversions of Chloroolefins over Iron Oxide Nanoparticles 1. Isomerization of Dichlorobutenes in the Presence of Iron Oxide Nanopaticles Immobilized on Silicas with Different Structures. *Russ. Chem. Bull.* **2005**, *54*, 1418–1424, doi:10.1007/s11172-005-0421-2.
36. Pankratov, D.A.; Yurev, A.I. Mössbauer Diagnostics of the Isomorphic Substitution of Iron for Aluminum in Triclinic Iron Vanadate. *Bull. Russ. Acad. Sci. Phys.* **2013**, *77*, 759–764, doi:10.3103/S1062873813060221.
37. Fysh, S.A.; Clark, P.E. A Mössbauer Study of the Iron Mineralogy of Acid-Leached Bauxite. *Hydrometallurgy* **1983**, *10*, 285–303, doi:10.1016/0304-386X(83)90060-9.
38. Janot, C.; Gibert, H. Les constituants du fer dans certaines bauxites naturelles étudiées par effet Mössbauer. *Bull. Société Fr. Minéralogie Cristallogr.* **1970**, *93*, 213–223, doi:10.3406/bulmi.1970.6456.
39. Vodyanitskii, Y.N.; Minkina, T.M.; Kubrin, S.P.; Pankratov, D.A.; Fedorenko, A.G. Common and Rare Iron, Sulfur, and Zinc Minerals in Technogenically Contaminated Hydromorphic Soil from Southern Russia. *Environ. Geochem. Health* **2020**, *42*, 95–108, doi:10.1007/s10653-019-00295-6.
40. Yurkov, G.Y.; Pankratov, D.A.; Koksharov, Yu.A.; Ovtchenkov, Ye.A.; Semenov, A.V.; Korokhin, R.A.; Shcherbakova, G.I.; Gorobinskiy, L.V.; Burakova, E.A.; Korolkov, A.V.; et al. Composite Materials Based on a Ceramic Matrix of Polycarbosilane and Iron-Containing Nanoparticles. *Ceram. Int.* **2022**, S0272884222032722, doi:10.1016/j.ceramint.2022.09.096.
41. Pankratov, D.A. Mössbauer Study of Oxo Derivatives of Iron in the Fe2O3-Na2O2 System. *Inorg. Mater.* **2014**, *50*, 82–89, doi:10.1134/S0020168514010154.
42. Betteridge, S.; Catlow, C.R.A.; Gay, D.H.; Grimes, R.W.; Hargreaves, J.S.J.; Hutchings, G.J.; Joyner, R.W.; Pankhurst, Q.A.; Taylor, S.H. Preparation, Characterisation and Activity of an Iron/Sodalite Catalyst for the Oxidation of Methane to Methanol. *Top. Catal.* **1994**, *1*, 103–110, doi:10.1007/BF01379580.
43. Krauss, K.; Höpke, A.; Mahn, M. *European Coatings journal*. 2019, pp. 36–42.
44. Levenspiel, O. *Chemical Reaction Engineering*; 3rd ed.; Wiley: New York, 1999; ISBN 978-0-471-25424-9.
45. Hidalgo, T.; Kuhar, L.; Beinlich, A.; Putnis, A. Kinetics and Mineralogical Analysis of Copper Dissolution from a Bornite/Chalcopyrite Composite Sample in Ferric-Chloride and Methanesulfonic-Acid Solutions. *Hydrometallurgy* **2019**, *188*, 140–156, doi:10.1016/j.hydromet.2019.06.009.
46. Koutsoupa, S.; Koutalidi, S.; Bourbos, E.; Balomenos, E.; Panias, D. Electrolytic Iron Production from Alkaline Bauxite Residue Slurries at Low Temperatures : Carbon-Free Electrochemical Process for the Production of Metallic Iron. *Johns. Matthey Technol. Rev.* **2021**, *65*, 366–374, doi:10.1595/205651320X15918757312944.
47. Liu, G.; Liu, Y.; Zhang, T. Approaches to Improve Alumina Extraction Based on the Phase Transformation Mechanism of Recovering Alkali and Extracting Alumina by the Calcification-Carbonization Method. *Hydrometallurgy* **2019**, *189*, 105123, doi:10.1016/j.hydromet.2019.105123.
48. Zhou, G.; Wang, Y.; Qi, T.; Zhou, Q.; Liu, G.; Peng, Z.; Li, X. Low-Temperature Thermal Conversion of Al-Substituted Goethite in Gibbsitic Bauxite for Maximum Alumina Extraction. *RSC Adv.* **2022**, *12*, 4162–4174, doi:10.1039/D1RA09013E.
49. Pankratov, D.A.; Anuchina, M.M.; Spiridonov, F.M.; Krivtsov, G.G. Fe3 – ΔO4 Nanoparticles Synthesized in the Presence of Natural Polyelectrolytes. *Crystallogr. Rep.* **2020**, *65*, 393–397, doi:10.1134/S1063774520030244.

50. Pankratov, D.A.; Anuchina, M.M. Nature-Inspired Synthesis of Magnetic Non-Stoichiometric Fe3O4 Nanoparticles by Oxidative in Situ Method in a Humic Medium. *Mater. Chem. Phys.* **2019**, *231*, 216–224, doi:10.1016/j.matchemphys.2019.04.022.
51. Bondarenko, L.S.; Pankratov, D.A.; Dzeranov, A.A.; Dzhardimalieva, G.I.; Streltsova, A.N.; Zarrelli, M.; Kydralieva, K.A. A Simple Method for Quantification of Nonstoichiometric Magnetite Nanoparticles Using Conventional X-Ray Diffraction Technique. *Mendeleev Commun.* **2022**, *32*, 642–644, doi:10.1016/j.mencom.2022.09.025.